Available online at www.sciencedirect.com
SCIENCE DIRECT®
Journal of Sound and Vibration 275 (2004) 605–621
JOURNAL OF SOUND AND VIBRATION
www.elsevier.com/locate/jsvi

Effects of rotation on the dynamics of a circular cylindrical shell with application to tire vibration ☆

Y.-J. Kim*, J.S. Bolton

Ray W. Herrick Laboratories, School of Mechanical Engineering, Purdue University, 140 South Intramural Drive, West Lafayette, IN 47907-2031, USA

Received 5 July 2002; accepted 26 June 2003

Abstract

For the purpose of understanding the effects of rotation on wave propagation within a tire's treadband, the vibration of an inflated, circular cylindrical shell, rotating about a fixed axis has been considered here. The equations of motion of the rotating shell are formulated in a fixed reference frame (i.e., Eulerian coordinates). By assuming wave-like solutions for the free vibration case, the natural frequencies and corresponding wave-like basis functions can then be obtained. A natural frequency selection procedure is introduced that can be used to associate each of the basis functions with a single natural frequency. The basis functions are then superimposed to represent the forced response of the system when driven by a point harmonic force at a fixed location in the reference frame. By using the procedure described here, the coefficients of the basis functions can be obtained directly by solving an uncoupled ordinary differential equation. Finally, the resulting forced responses are presented in both the spatial and wave number domains, and the wave number spectrum of the rotating shell is compared with that of a stationary shell. Based on the results presented here, it is suggested that at typical rotational speeds it may be possible to use a stationary tire analysis to predict the characteristics of a rotating tire after performing a simple kinematic compensation.

1. Introduction

In two previous articles, the stationary-tire dispersion relations that characterize a tire's dynamics and its potential for sound radiation were considered [1,2]. The first article described both an experimental measurement procedure and a wave number decomposition technique for

☆A shorter version of this article was presented at INTER-NOISE 2002.

*Corresponding author. Tel.: +1-765-494-2139; fax: +1-765-494-0787.
E-mail address: kimyj1@purdue.edu (Y.-J. Kim).

0022-460X/$ - see front matter © 2003 Elsevier Ltd. All rights reserved.
doi:10.1016/j.jsv.2003.06.003

analyzing the radial vibration of a tire. In the second article, analytical and numerical models of tire treadbands that were found to reproduce the significant features of measured tire dispersion relations were described. The objective of the work described in the present article was to extend the earlier analytical model to determine the effects of rotation on a tire's dispersion relations. For this purpose, a tire treadband has been modelled as a simply supported, rotating circular cylindrical shell. Both inflation pressure and rotational stiffening were accounted for in the model.

2. Background

In a rotating shell, a moving particle whose motion is described in local co-ordinates that rotate with the shell is subject to Coriolis acceleration. As a result, the circumferential phase speeds of the pair of positive- and negative-going waves in the local co-ordinates differ from each other (when the shell is stationary, they are identical regardless of the wave propagation direction). The latter difference is also observed when the shell motion is described in fixed reference co-ordinates (i.e., Eulerian co-ordinates), since, in addition to the effects of Coriolis acceleration, the circumferential phase speed of the positive-going wave increases by the rotation speed, while that of the corresponding negative-going wave decreases by the same amount. Since the natural frequency associated with a particular circumferentially propagating wave can be related to both the circumferential wave number and the circumferential phase speed, the natural frequency associated with the positive-going wave in the rotating shell is different from that associated with the corresponding negative-going wave. Consequently, a single natural frequency that in the stationary shell case is associated with a pair of positive- and negative-going waves splits into two natural frequencies when the shell rotates. That is, in the stationary shell, the positive- and negative-going waves interfere with each other at a single natural frequency to yield a circumferential standing wave pattern (i.e., mode shape); however, in the rotating case, a standing wave pattern cannot be generated at a single natural frequency.

When a rotating shell is analyzed by using a circumferential mode shape represented by a circumferential sine or cosine function, the pair of natural frequencies associated with that mode shape can be found; however, the natural frequencies cannot be associated with a particular circumferentially propagating wave direction. Since the set of mode shapes represented by the circumferential sine and cosine functions is a complete set, as is the set of wave-like basis functions represented by the circumferential complex exponential functions (i.e., positive- and negative-going waves), the forced response can be represented with equal accuracy by the superposition of either the mode shapes or complex exponential functions. However, the modal solution procedure requires one to solve the complete system differential equations to determine the modal coefficients since a pair of circumferential sine and cosine mode shapes share two natural frequencies (i.e., the modal coefficients are coupled with each other) [3–5]. Note that the circumferential mode number, n, must be an integer due to circular periodicity; thus, to obtain a complete set of circumferential sine and cosine functions, n should range from zero to positive infinity, while a complete set of circumferential complex exponential functions is obtained by allowing n to range from negative to positive infinity [6].

Padovan obtained the complete set of natural frequencies and corresponding mode shapes for rotating, prestressed circular cylindrical shells [6]. By using those natural modes, Huang and

Soedel obtained the forced response of a rotating ring, a special case of a rotating circular cylindrical shell (i.e., no spatial variation was allowed in the axial direction) [3,4]. Note that a ring model can be used to analyze the vibrational characteristics of a rotating tire; however, such a model cannot account for the effects of the cross-sectional modes (in the axial direction). Note also that Kropp has modelled a stationary tire as a stationary ring [7].

Forced solutions for the case of a rotating, prestressed circular cylindrical shell were previously obtained by Huang and Soedel [5]. They expressed their forced responses in terms of sinusoidal and cosinusoidal modes; however, only circumferential sine *or* cosine functions were used to represent the forced responses, and the $n = 0$ circumferential mode (i.e., the breathing mode), that can be important in terms of sound radiation, was not considered. Unless the shell's motion is represented as a sum of both circumferential sine and cosine functions, including the $n = 0$ circumferential mode, spatial phase information in the circumferential direction cannot be represented accurately. Note, however, that in two earlier papers dealing with rotating rings, Huang and Soedel used a complete set of modes [3,4].

In the past, the equations of motion and the solutions for rotating shells were mainly formulated in a local co-ordinate system [3–6]. However, that type of formulation creates difficulties when applying a sinusoidal point force at a fixed point to simulate a contact patch excitation of a rotating tire since, in the local frame, the response is Doppler shifted. In contrast, a system described in fixed reference co-ordinates, as here, responds at the frequency of the input force.

Another approach to representing the effects of tire rotation was followed by Vinesse and Nicollet, who modelled a tire as a two-dimensional membrane [8]. They derived the equations of motion in a fixed reference frame, and obtained continuous dispersion curves, each associated with a particular cross-sectional mode shape, by using a wave-like solution (expressed in terms of a continuously varying circumferential wave number). They also obtained an approximate forced response, which was expressed as a function of time and circumferential position (but not as a function of cross-sectional position), for the case of a rotating point force. In their work, however, effects of flexural stiffness and circumferential curvature were neglected, and in-plane motion was not allowed.

Here, it was decided to express the equations of motion for the case of a rotating, inflated circular cylindrical shell in fixed reference co-ordinates since the forced response in fixed reference co-ordinates can be used directly to perform a sound radiation analysis. A wave-like basis solution, which comprises a mode shape in the cross-sectional direction (i.e., axial direction) and a wave-like solution in the circumferential direction, was then used to obtain the complete sets of natural frequencies and corresponding basis functions (the cross-sectional mode shape is represented by sine and cosine functions, and the circumferential wave-like solution is expressed by a complex exponential function). Here, a natural frequency selection procedure that can be used to associate each wave-like basis function with a single natural frequency is proposed. By the superposition of the basis functions, the forced response of the system can be obtained when the system is driven by a point harmonic force at a fixed location in the reference frame. Since a single basis function is associated with only one natural frequency, a basis function coefficient can be found by solving a single ordinary differential equation. In addition, the wave number decomposition procedure [1] has been applied to the resulting forced responses, thus allowing the dispersion relations for a rotating shell to be represented from the viewpoint of a

fixed observer so that they can be easily compared with the dispersion relations for a stationary shell.

3. Tire treadband model

Fig. 1 shows a cylindrical shell model of a tire treadband: the shell is assumed to rotate about a fixed axis coincident with the origin of the reference co-ordinate system. Note that the local co-ordinate system, attached to the treadband, rotates with the treadband and that the reference co-ordinate system is fixed. In the present analysis, the effects of inflation pressure and rotational stiffening were accounted for through resultant in-plane residual stresses. However, static deformation of the shell due to either inflation or rotation was neglected, i.e., the treadband was assumed to vibrate around its static, uninflated shape.

When shear deformation, rotary inertia, and non-linear effects are neglected, a set of equations describing the three-dimensional motion of the shell can be derived in local co-ordinates [9]. Those equations can be transformed into the reference co-ordinate system by application of Reynolds' theorem, i.e.,

$$\frac{\mathrm{D}}{\mathrm{D}t} = \frac{\partial}{\partial t} + \Omega \frac{\partial}{\partial \phi}, \tag{1}$$

where the left hand side represents the time derivative in the local (Lagrangian) co-ordinates, the first term on the right hand side is the time derivative in the reference (Eulerian) co-ordinates, Ω is the angular rotational speed and ϕ is the circumferential angle in the reference frame. After applying Eq. (1), the governing equations can be expressed as

$$L_x(u_x, u_\phi, u_r) + \lambda \frac{\mathrm{D}u_x}{\mathrm{D}t} + \rho h \frac{\mathrm{D}^2 u_x}{\mathrm{D}t^2} = q_x(x, \phi, r), \tag{2}$$

$$L_\phi(u_x, u_\phi, u_r) + \lambda \frac{\mathrm{D}u_\phi}{\mathrm{D}t} + \rho h \left(\frac{\mathrm{D}^2 u_\phi}{\mathrm{D}t^2} + 2\Omega \frac{\mathrm{D}u_r}{\mathrm{D}t} - \Omega^2 u_\phi \right) = q_\phi(x, \phi, r), \tag{3}$$

$$L_r(u_x, u_\phi, u_r) + \lambda \frac{\mathrm{D}u_r}{\mathrm{D}t} + \rho h \left(\frac{\mathrm{D}^2 u_r}{\mathrm{D}t^2} - 2\Omega \frac{\mathrm{D}u_\phi}{\mathrm{D}t} - \Omega^2 u_r \right) = q_r(x, \phi, r), \tag{4}$$

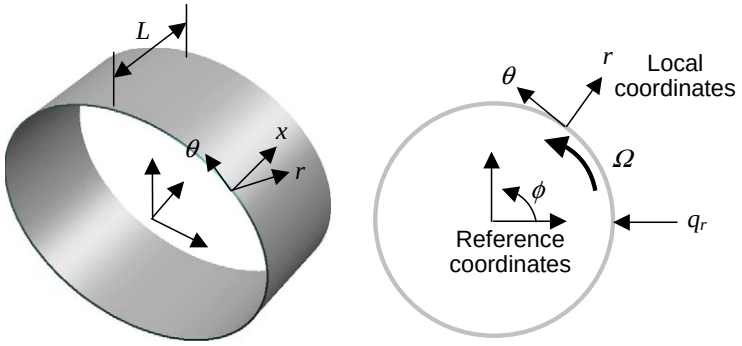

Fig. 1. Model of tire treadband: a circular cylindrical shell with simply supported edges.

$$L_x(u_x, u_\phi, u_r) = -\frac{\partial N_{xx}}{\partial x} - \frac{1}{a}\frac{\partial N_{\phi x}}{\partial \phi}, \tag{5}$$

$$L_\phi(u_x, u_\phi, u_r) = -\frac{\partial N_{x\phi}}{\partial x} - \frac{\partial N_{\phi\phi}}{\partial \phi} - \frac{Q_{\phi r}}{a}, \tag{6}$$

$$L_r(u_x, u_\phi, u_r) = -\frac{\partial Q_{xr}}{\partial x} - \frac{1}{a}\frac{\partial Q_{\phi r}}{\partial \phi} + \frac{N_{\phi\phi}}{a} - N^r_{xx}\frac{\partial^2 u_r}{\partial x^2} - \frac{N^r_{\phi\phi}}{a^2}\frac{\partial^2 u_r}{\partial \phi^2}, \tag{7}$$

where u is the displacement in the direction indicated by the subscript, N_{ij} and Q_{ij} ($i, j = x, \phi, r$) are the resultant in-plane and shear forces (see Appendix A), respectively, the superscript, r, denotes residual force, and q is the external force applied in the direction indicated by the subscript. In addition, ρ is the density of the treadband, h is its thickness, λ is the damping constant, and a is the tire radius. In Eq. (7), the circumferential resultant in-plane force is related to inflation pressure and rotational speed by

$$N^r_{\phi\phi} = ap + \rho h a^2 \Omega^2, \tag{8}$$

where p is the inflation pressure [9].

The linear operators, L_i ($i = x, \phi, r$), are associated with the system's stiffness and thus Eqs. (7) and (8) indicate how inflation pressure and rotation affect the treadband's stiffness. When the magnitudes of the two terms on the right hand side of Eq. (8) are compared, it can be concluded that stiffening effects associated with rotation may be ignored compared to the stiffening effect of inflation pressure at speeds typical of those experienced by a car tire running at normal speeds, at least for the model considered here. The latter result will be demonstrated by calculation later in this article.

4. Natural vibration

Simple support conditions were considered to apply constraints in the radial and circumferential, but not the x direction, at the treadband edges. In that case, a set of displacements satisfying those boundary conditions, i.e., sinusoidal or cosinusoidal functions in the x direction, as appropriate, can be identified [5,9]. That set must also be periodic in the circumferential direction. Based upon these various conditions, the set of displacements were assumed to have the wave-like forms

$$u_{xmn}(x, \phi, t) = A_{mn}\cos\left(\frac{m\pi x}{L}\right)\exp(\mathrm{i}\omega_{mn}t - \mathrm{i}n\phi), \tag{9}$$

$$u_{\phi mn}(x, \phi, t) = \mathrm{i}B_{mn}\sin\left(\frac{m\pi x}{L}\right)\exp(\mathrm{i}\omega_{mn}t - \mathrm{i}n\phi), \tag{10}$$

$$u_{rmn}(x, \phi, t) = C_{mn}\sin\left(\frac{m\pi x}{L}\right)\exp(\mathrm{i}\omega_{mn}t - \mathrm{i}n\phi), \tag{11}$$

where the coefficients A, B and C are assumed to be real. By substituting Eqs. (9)–(11) into Eqs. (2)–(4), and setting the input force and damping to zero, a matrix equation similar to that

defining an eigenvalue problem can be obtained, i.e.,

$$\begin{bmatrix} k_{11}-\rho h\varpi_{mn}^2 & k_{12} & k_{13} \\ k_{12} & k_{22}-\rho h(\varpi_{mn}^2+\Omega^2) & k_{23}+2\rho h\Omega\varpi_{mn} \\ k_{13} & k_{23}+2\rho h\Omega\varpi_{mn} & k_{33}-\rho h(\varpi_{mn}^2+\Omega^2) \end{bmatrix} \begin{bmatrix} A_{mn} \\ B_{mn} \\ C_{mn} \end{bmatrix} = \begin{bmatrix} 0 \\ 0 \\ 0 \end{bmatrix}, \tag{12}$$

where

$$\varpi_{mn} = \omega_{mn} - n\Omega, \tag{13}$$

$$k_{11} = K\left[\left(\frac{m\pi}{L}\right)^2 + \frac{1-\nu}{2}\left(\frac{n}{a}\right)^2\right], \tag{14}$$

$$k_{12} = -K\frac{1+\nu}{2}\left(\frac{m\pi}{L}\right)\left(\frac{n}{a}\right), \tag{15}$$

$$k_{13} = -\frac{K\nu}{a}\left(\frac{m\pi}{L}\right), \tag{16}$$

$$k_{22} = \left(K+\frac{D}{a^2}\right)\left[\frac{1-\nu}{2}\left(\frac{m\pi}{L}\right)^2 + \left(\frac{n}{a}\right)^2\right], \tag{17}$$

$$k_{23} = \frac{nK}{a^2} + \frac{nD}{a^2}\left[\left(\frac{m\pi}{L}\right)^2 + \left(\frac{n}{a}\right)^2\right] \tag{18}$$

and

$$k_{33} = D\left[\left(\frac{m\pi}{L}\right)^2 + \left(\frac{n}{a}\right)^2\right]^2 + \frac{K}{a^2} + N_{xx}^r\left(\frac{m\pi}{L}\right)^2 + N_{\phi\phi}^r\left(\frac{n}{a}\right)^2. \tag{19}$$

In Eq. (12), the stiffness terms, k_{ij} $(i,j=1,2,3)$, are associated with the linear operators, L_i $(i=x,\phi,r)$, and they are given in Eqs. (14)–(19), where K is the membrane stiffness, D is the bending stiffness, and ν is the Poisson ratio. Here, the membrane stiffness is $K=Eh/(1-\nu^2)$ and the bending stiffness is $D=Eh^3/[12(1-\nu^2)]$, where E is Young's modulus. Further, in Eq. (13) the left hand side is the natural frequency in local co-ordinates while the first term on the right hand side is the natural frequency in the reference co-ordinate system. For future reference, Eq. (13) will be referred to as the "kinematic relation".

The characteristic equation obtained from Eq. (12) is sixth order, i.e., there are six natural frequencies associated with the (m,n)th wave-like solution. However, the six local natural frequencies, of the negative-going, i.e., $(m,-n)$ wave-like solutions, where $n>0$, each have the same magnitude but opposite sign of those of the positive-going (m,n) wave-like solutions. Thus, when a local natural frequency is defined to be positive, the sign convention used in the assumed displacements (see Eqs. (9)–(11)) means that a positive n denotes a positive-going wave and a negative n a negative-going wave. Thus, for each positive or negative n, the three positive local natural frequencies are chosen and the negative natural frequencies are discarded. There are then only three distinct local natural frequencies associated with each (m,n) wave mode, whether $n>0$ or $n<0$. Each of those frequencies is primarily associated with a particular wave type, i.e., flexural, longitudinal, or shear [2]. Note that the two local natural frequencies associated with the

pair of wave-like basis functions propagating in opposite circumferential directions are different even in the local frame owing to the effects of Coriolis acceleration, as will be shown later: this phenomenon is referred to as "bifurcation" [6].

The natural frequencies for all possible combinations of m and n (for both positive and negative n) can be found by numerically solving the characteristic equation derived analytically from Eq. (12). By applying the sign convention described above, the three distinct natural frequencies associated with each n can then be identified. The associated vectors represented by $[A_{mnl}\ B_{mnl}\ C_{mnl}]^{\mathrm{T}}$, where the index l ($l = 1-3$) denotes the three natural frequencies for each n, can also be derived by using Eq. (12): i.e., the three sets of vectors can be calculated by substituting each of the natural frequencies in sequence into Eq. (12). As a result, a single natural frequency, ω_{mnl}, can be associated with a particular wave-like basis vector function represented by

$$\mathbf{\Psi}_{mnl}(x,\phi) = \begin{bmatrix} A_{mnl}\cos\left(\dfrac{m\pi x}{L}\right) \\ \mathrm{i}B_{mnl}\sin\left(\dfrac{m\pi x}{L}\right) \\ C_{mnl}\sin\left(\dfrac{m\pi x}{L}\right) \end{bmatrix} \exp(-\mathrm{i}n\phi). \tag{20}$$

5. Forced vibration

The forced response can be expressed as a superposition of the basis functions given in Eq. (20), i.e.,

$$u_x(x,\phi,t) = \sum_{m=1}^{\infty}\sum_{n=-\infty}^{\infty}\sum_{l=1}^{3} A_{mnl}\cos\left(\frac{m\pi x}{L}\right)\exp(-\mathrm{i}n\phi)\eta_{mnl}(t), \tag{21}$$

$$u_\phi(x,\phi,t) = \sum_{m=1}^{\infty}\sum_{n=-\infty}^{\infty}\sum_{l=1}^{3} \mathrm{i}B_{mnl}\sin\left(\frac{m\pi x}{L}\right)\exp(-\mathrm{i}n\phi)\eta_{mnl}(t) \tag{22}$$

and

$$u_r(x,\phi,t) = \sum_{m=1}^{\infty}\sum_{n=-\infty}^{\infty}\sum_{l=1}^{3} C_{mnl}\sin\left(\frac{m\pi x}{L}\right)\exp(-\mathrm{i}n\phi)\eta_{mnl}(t). \tag{23}$$

Note that for the purpose of compactness, the index, mnl is replaced by k in the following equations. The weighting function (i.e., the coefficient of the basis function), $\eta_k(t)$, can be calculated by substituting Eqs. (21)–(23) into Eqs. (2)–(4) and then applying Eqs. (12) and (13) with damping and forcing terms included. The result is

$$\ddot{\eta}_k + \left(\frac{\lambda_k}{\rho h} - \mathrm{i}2\Omega(n+2\gamma_k)\right)\dot{\eta}_k + \left(\omega_k^2 - 2\Omega\omega_k(n+2\gamma_k) - \mathrm{i}n\Omega\frac{\lambda_k}{\rho h}\right)\eta_k = \frac{F_k}{\rho h W_k}, \tag{24}$$

where

$$W_k = \pi L(A_k^2 + B_k^2 + C_k^2), \quad \gamma_k = \frac{B_k C_k}{A_k^2 + B_k^2 + C_k^2} \tag{25, 26}$$

and

$$F_k = \int_0^{2\pi} \int_0^L \left[q_x A_k \cos\left(\frac{m\pi x}{L}\right) + \mathrm{i} q_\phi B_k \sin\left(\frac{m\pi x}{L}\right) + q_r C_k \sin\left(\frac{m\pi x}{L}\right) \right] \mathrm{e}^{\mathrm{i}n\phi} \mathrm{d}x \, \mathrm{d}\phi. \tag{27}$$

Eq. (24) may then be solved to give $\eta_k(t)$ for arbitrary temporal input forces. Note that the modal damping constant, λ_k, in Eq. (24) is here expressed in terms of a constant modal damping ratio, ξ, and the natural frequency, ω_k, as

$$\lambda_k = 2\rho h \xi \omega_k. \tag{28}$$

Note also that the coefficient of the basis function can be found directly by solving the ordinary differential equation, Eq. (24).

Next, consider a harmonic point force applied in the radial direction at a fixed point while the forces in the other directions are assumed to be zero (i.e., $q_x = 0$ and $q_\phi = 0$). This radial force applied at the center of the treadband simulates a contact patch excitation of a rotating tire and it can be expressed as

$$q_r(x, \phi, t) = f_0 \delta\left(x = \frac{L}{2}, \phi = 0\right) \exp(\mathrm{i}\omega t), \tag{29}$$

where f_0 is the constant amplitude of the force and δ is the Dirac delta function. Given a harmonic force as expressed in Eq. (29), the kth response function, $\eta_k(t)$, can also be expressed in harmonic exponential form, i.e.,

$$\eta_k(t) = X_k \exp(\mathrm{i}\omega t), \tag{30}$$

where X_k is the amplitude of the kth basis function. By substituting Eqs. (29) and (30) into Eqs. (24)–(28), the amplitude is obtained as

$$X_k = \frac{f_0 C_k \sin(m\pi/2)}{\rho h W_k [\omega_k^2 - \omega^2 - 2\Omega(n + 2\gamma_k)(\omega_k - \omega) + \mathrm{i}2(\omega - n\Omega)\omega_k \xi]}. \tag{31}$$

6. Results and discussion

The tire treadband parameters used for the calculation presented here are listed in Table 1: they were adapted from Ref. [7], were based on physical reasoning, or were obtained by direct measurement of tires.

Fig. 2 shows the dispersion relations obtained by solving the system characteristic equation for each combination of m and n; the dispersion relations are therefore defined at a set of discrete points. Note that the x-axis of Fig. 2 and the following is the circumferential wave number, k_ϕ, which is related to the circumferential mode number, n, by $k_\phi = n/a$. In Fig. 2, each trajectory of the dispersion relation is associated with a particular cross-sectional mode index, i.e., $m = 1$, etc. as shown in Fig. 2(a).

For each combination of m and n, there are three natural frequencies associated primarily with flexural, shear, and longitudinal motions in order of increasing frequency [2]. The stationary dispersion relations are plotted in Fig. 2(a). In Fig. 2(b), the local natural frequencies are plotted when the rotation speed was set to the artificially large value of $\Omega = 500$ rad/s to exaggerate the effects of rotation: a more typical range for automotive applications is from $\Omega = 0$ to 100 rad/s.

Table 1
Parameters for tire treadband

Young's modulus	$E = 4.8 \times 108\,\mathrm{N/m^2}$
Density	$\rho = 1200\,\mathrm{kg/m^3}$
Thickness	$h = 0.008\,\mathrm{m}$
Poisson ratio	$v = 0.45$
Radius	$a = 0.32\,\mathrm{m}$
Width	$L = 0.16\,\mathrm{m}$
Damping ratio	$\xi = 0.05$
Inflation pressure	$p = 206910\,\mathrm{Pa}$ ($p = 30$ psi)
Sidewall tension	$N^r_{xx} = 2 \times 10^4\,\mathrm{N/m}$

By comparison of Fig. 2(b) with Fig. 2(a), two phenomena can be observed. First, it can be seen that the speed of the flexural waves is increased by rotational stiffening (i.e., the slope of the flexural modal trajectories is increased.). In contrast, the change of the speeds of the shear and longitudinal waves is essentially negligible. Secondly, on close examination, it can be seen that rotation causes the dispersion curves to be very slightly asymmetrical with respect to the zero wave number axis: this is the so-called "bifurcation" effect. The latter asymmetry means that the speeds of waves propagating in opposite circumferential directions with the same wavelengths are different even when observed in the local co-ordinate system. However, the present results indicate that this effect is negligible for the model considered here under normal circumstances (see Fig. 2(c)). Results in local co-ordinates for a more typical rotational speed, $\Omega = 100\,\mathrm{rad/s}$, are plotted in Fig. 2(c). By comparison with the $\Omega = 0$ results in Fig. 2(a), it can be seen that the stiffening due to rotation is not very significant in this case, as explained earlier in connection with Eq. (8).

Finally, the dispersion relations in the reference frame are plotted in Fig. 2(d), also for $\Omega = 100\,\mathrm{rad/s}$. Note that the latter results were obtained from those of Fig. 2(c) by applying the kinematic relation, Eq. (13). In Fig. 2(d), the asymmetry resulting from the kinematic effect of tire rotation is very clear in contrast with the bifurcation effect in local co-ordinates (Fig. 2(c)).

For the purpose of validating the modelling and solution procedures, the stationary model ($\Omega = 0$) was reproduced by using a FE model [2]. The corresponding wave number-transformed forced solutions (presented as radial velocity magnitudes) for a radial point force on the treadband center-line calculated using FE and analytical procedures are plotted in Fig. 3. The two results are identical for practical purposes.

The spatial distributions of the center-line radial velocities for a fixed-location radial point force applied on the shell center-line are plotted at selected frequencies in the reference frame in Fig. 4, and the complete set of results, along with the corresponding circumferentially wave number-transformed results are shown in Fig. 5. Note that 0° in Figs. 4 and 5(a) indicates the drive point. One interesting aspect of these results is that clear stationary wave patterns (with respect to the fixed frame) appear even under rotation. In a sense, the stationary waves are strengthened by damping, since the latter causes the dispersion trajectories to be broader, thus making it more likely that there will be wave components propagating in opposite directions with the same wavelength at the same frequency. It can also be seen in Fig. 4 that the rate of decay with distance increases as the damping ratio is increased (cf. Figs. 4(a) and (b)) and that the effect of damping

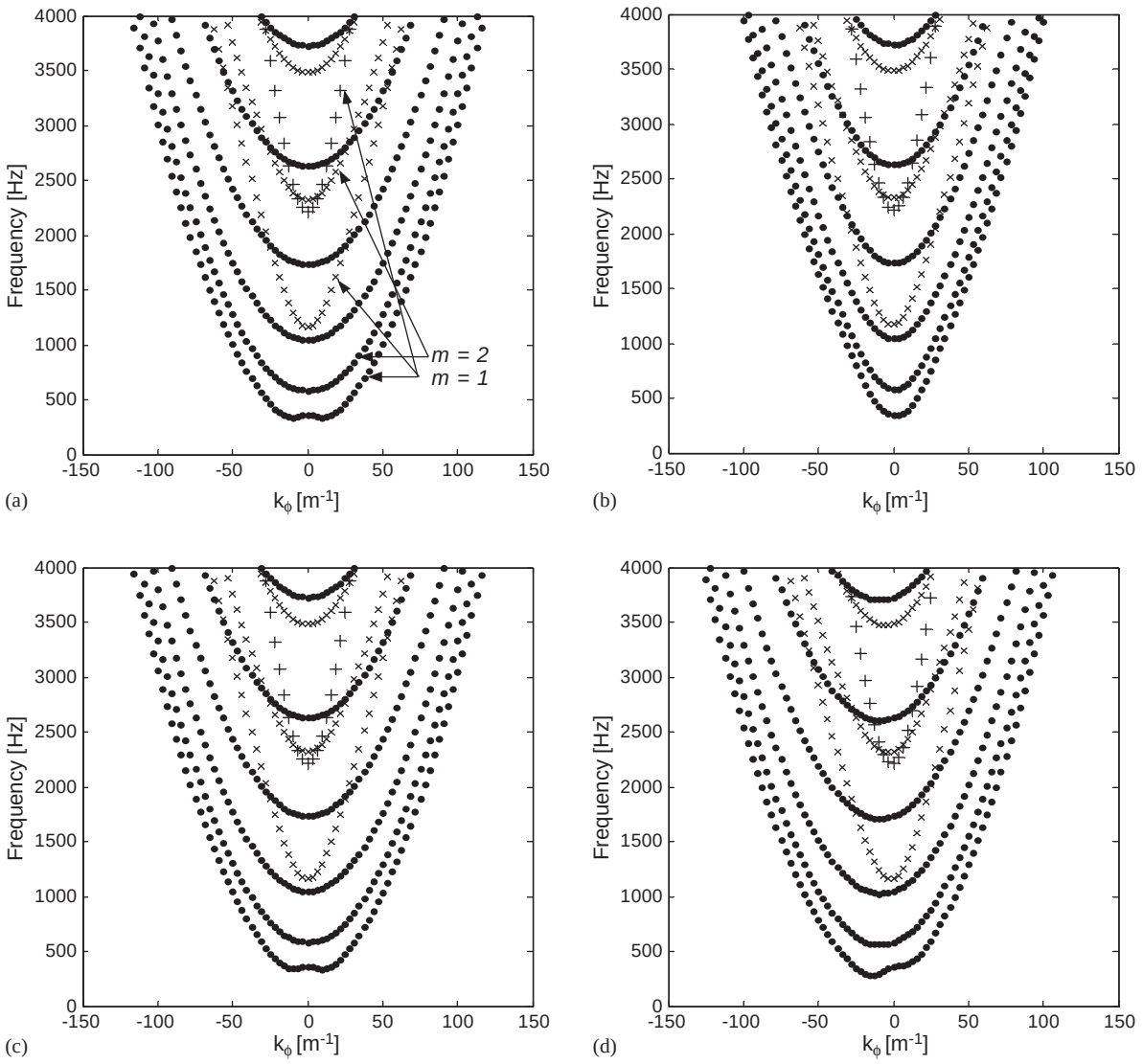

Fig. 2. Dispersion relations derived from characteristic equation: •, flexural wave, ×, shear wave, and +, longitudinal wave. (a) Natural frequencies when $\Omega = 0$, (b) natural frequencies in local co-ordinates when $\Omega = 500$ rad/s, (c) natural frequencies in local co-ordinates when $\Omega = 100$ rad/s, and (d) natural frequencies in reference co-ordinates when $\Omega = 100$ rad/s.

increases with frequency. Thus, at high frequencies the response becomes similar to a free-field response as the damping is increased: e.g., at $f = 3200$ Hz, $\xi = 0.05$, the response level drops by approximately 40 dB by half-way around the treadband. The latter result is consistent with measurements made on stationary tires [1,10]. Further, a comparison of the responses in the positive- and negative-ϕ regions of Fig. 4 (i.e., in the upstream and downstream directions, respectively) shows that the levels are generally higher in the downstream direction. The latter effect becomes clearer as the rotational speed increases (cf. Figs. 4(b) and (c)). These various

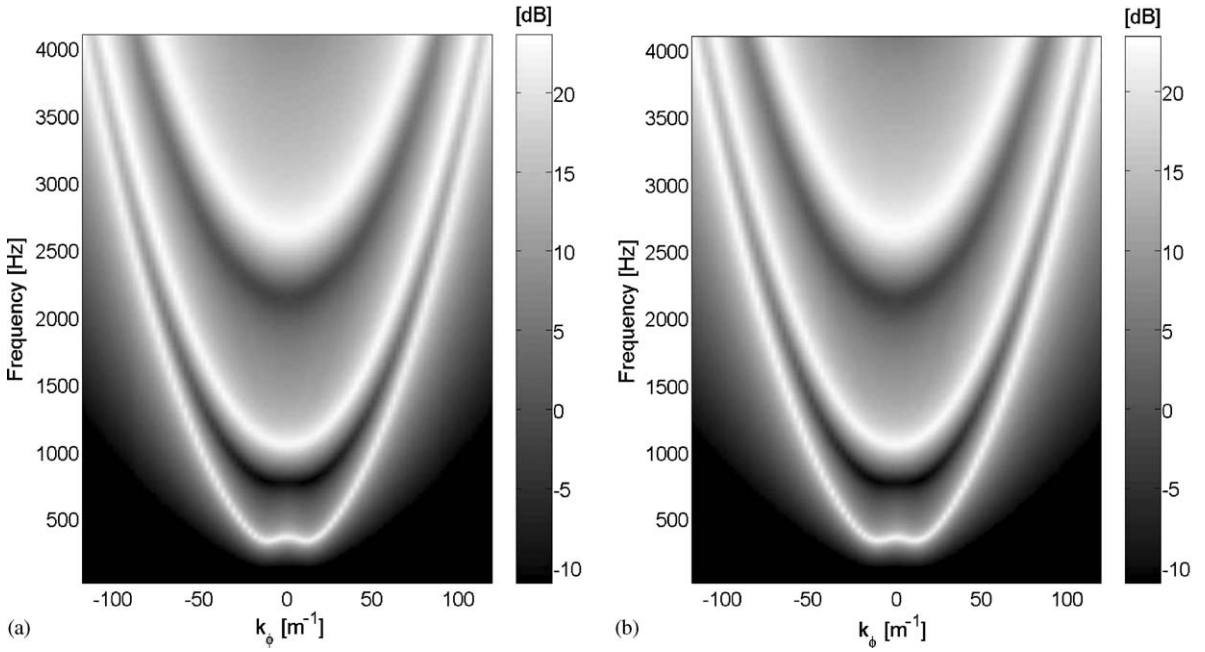

Fig. 3. Comparison of analytical forced response (radial velocity) with FE simulation when $\Omega = 0$ rad/s and $\xi = 0.05$: (a) FE simulation and (b) analytical solution.

effects can also be seen in Fig. 5(a). In the higher frequency region of Fig. 5(a) it is also clear that several wave modes, each having different wavelengths, contribute significantly to the response simultaneously. The latter is also clear in the wave number-transformed results shown in Fig. 5(b). It can also be seen that the even cross-sectional modes (i.e., $m = 2,4,6,\ldots$) are absent from the results of Fig. 5(b) (compare with Fig. 2(d)) since the point force was applied at the center of treadband. Also note that the trajectories in Fig. 5(b) are continuous (not discrete, as in Fig. 2), in part because of the effect of damping. The asymmetry of the trajectory slopes in Fig. 5(b) also indicates that waves travel more quickly downstream ($k_\phi > 0$) than upstream, as expected.

Finally, the input point mobility, $i\omega u_r/q_r$, associated with the negative- and positive-going wave components is shown in Fig. 6. The results were calculated by summing Eq. (23) separately over positive and negative n, and assigning half of the $n = 0$ component to each summation. The mobility associated with the positive-going (i.e., downstream) components is generally larger than that associated with the negative-going components (except near the cut-on frequencies of progressively higher order cross-sectional modes) which is consistent with the relative magnitudes of the responses in the up- and downstream sections shown in Fig. 4. The sequence of small peaks in the mobility from approximately 400 to 900 Hz (most clearly visible in the positive-going result) are related to the circumferential modes associated with the first cross-sectional mode ($m = 1$). The contributions of individual modes are not easily visible in the frequency ranges above the cut-on frequencies of the $m = 3$ and 5 cross-sectional modes (near 1000 and 2600 Hz, respectively). The latter observation is also consistent with measured results for tires [10].

Since both the rotational stiffness and bifurcation effects are essentially negligible under the conditions considered here, it is possible to map the stationary forced response (Fig. 3(b)) onto the

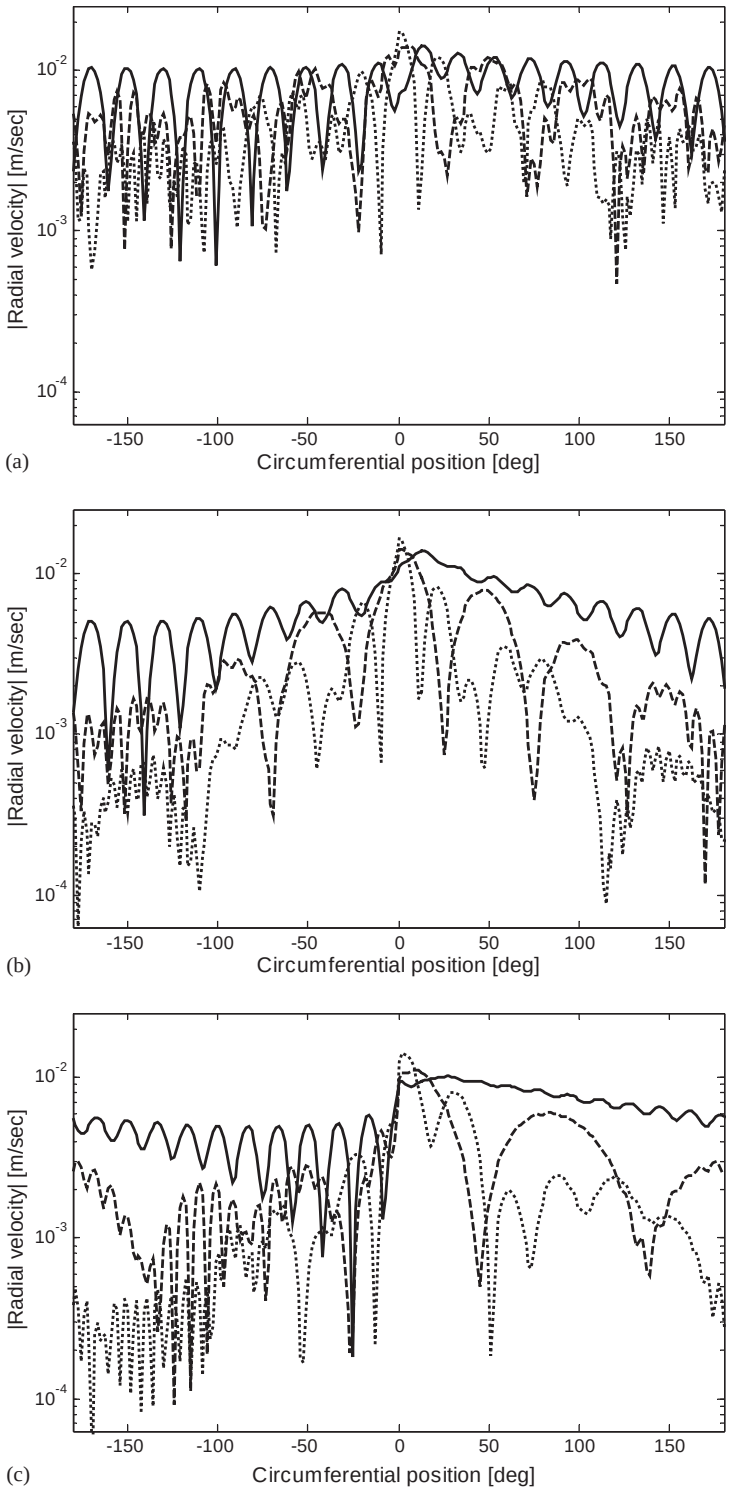

Fig. 4. Forced responses at 512 Hz (solid line), 1600 Hz (dashed line), and 3200 Hz (dotted line): (a) Ω= 100 rad/s and $\xi = 0.02$, (b) $\Omega = 100$ rad/s and $\xi = 0.05$, and (c) Ω= 500 rad/s and $\xi = 0.05$.

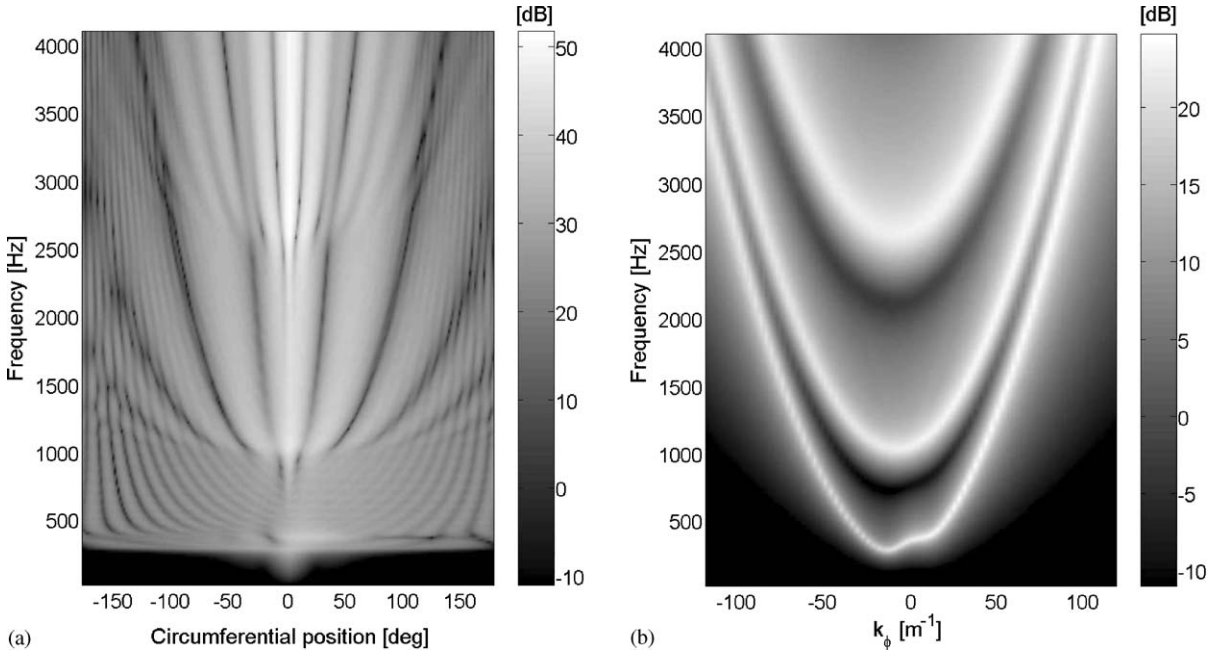

Fig. 5. Forced response when $\Omega = 100$ rad/s and $\xi = 0.05$: (a) magnitude of vibration (radial velocity) at treadband center and (b) dispersion relation obtained by circumferential wave number transform.

rotational response by using Eq. (13) when the local natural frequency is assumed to be the natural frequency of the stationary tire. In the latter case, Eq. (13) can be modified to compensate for rotational effects in the wave number-frequency domain, i.e.,

$$f = f_s + \frac{k_\phi a}{2\pi}\Omega, \tag{32}$$

where f and f_s are the rotation-compensated and stationary tire natural frequencies, respectively.

For the purpose of validating Eq. (32), parametric representations of the dispersion relations were obtained first by applying the Prony series procedure described in Ref. [1]: the resulting real wave numbers are overlaid on the previous results (Figs. 3(b) and 5(b)) in Fig. 7. It can be seen that the real wave numbers thus identified lie on the local maxima of the dispersion relations obtained by application of the spatial Fourier transform. The stationary real wave numbers of Fig. 7(a) were then modified by applying Eq. (32) to compensate for rotational effects: the results are shown in Fig. 8 along with the direct results for the rotational case. It can be seen that the compensated stationary dispersion relations are essentially identical with those of the rotational case.

7. Conclusion

In the work described here, the treadband of a tire was modelled as an inflated, rotating circular cylindrical shell in order to identify the effects of rotation. A wave-based solution procedure was

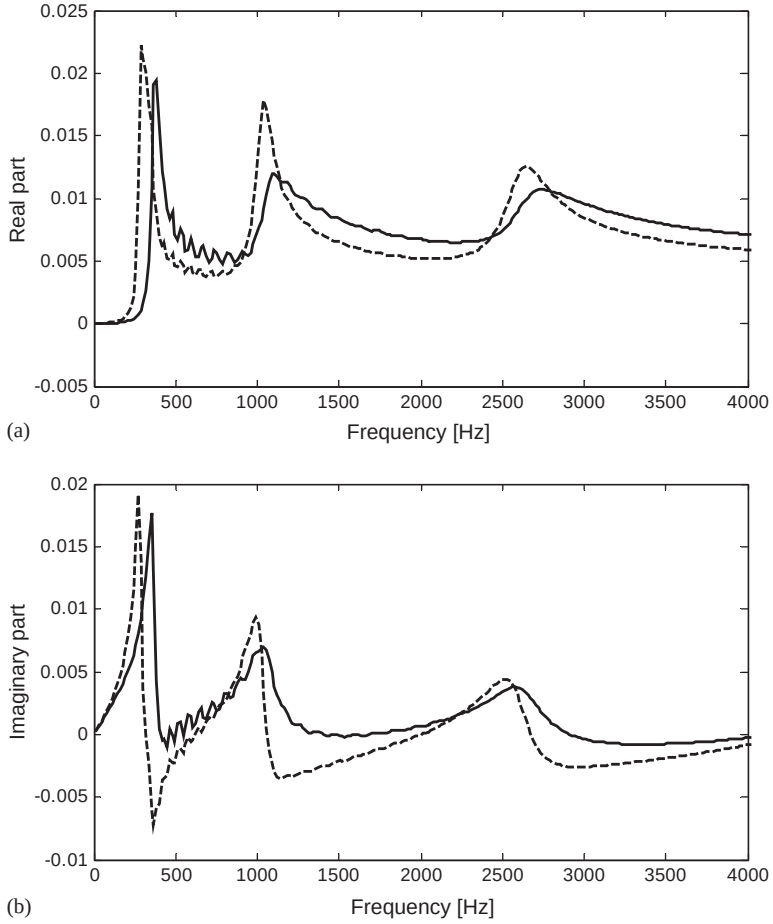

Fig. 6. Input point mobility, $i\omega ur/qr$. Solid line indicates modal summation of positive-going wave components ($n > 0$) and half of $n = 0$ component, and dashed line indicates negative-going wave components ($n < 0$) and half of $n = 0$ component: (a) real part and (b) imaginary part.

used to obtain analytical solutions for both free and forced vibration cases. In particular, it was shown that a natural frequency selection procedure described here could be used to select the natural frequencies based on circumferentially propagating wave characteristics in the rotating shell. Additionally, the forced solutions were obtained by the superposition of wave-like basis functions: in the latter procedure, the superposition coefficient could be determined by solving an uncoupled ordinary differential equation.

The results presented here show that rotation has two principal effects: stiffening of the treadband and kinematic "tilting" of the dispersion curves. It was found, however, that the rotational stiffening effect was not significant compared with the effect of inflation pressure, for the model considered here, at typical rotational speeds. In contrast, the kinematic tilting effect was found to be significant. Thus, it was concluded that a linear function, Eq. (32), could be used to adjust stationary shell dispersion curves for the effects of rotation: the latter curves may then be used to analyze the potential of a rotating tire to radiate sound.

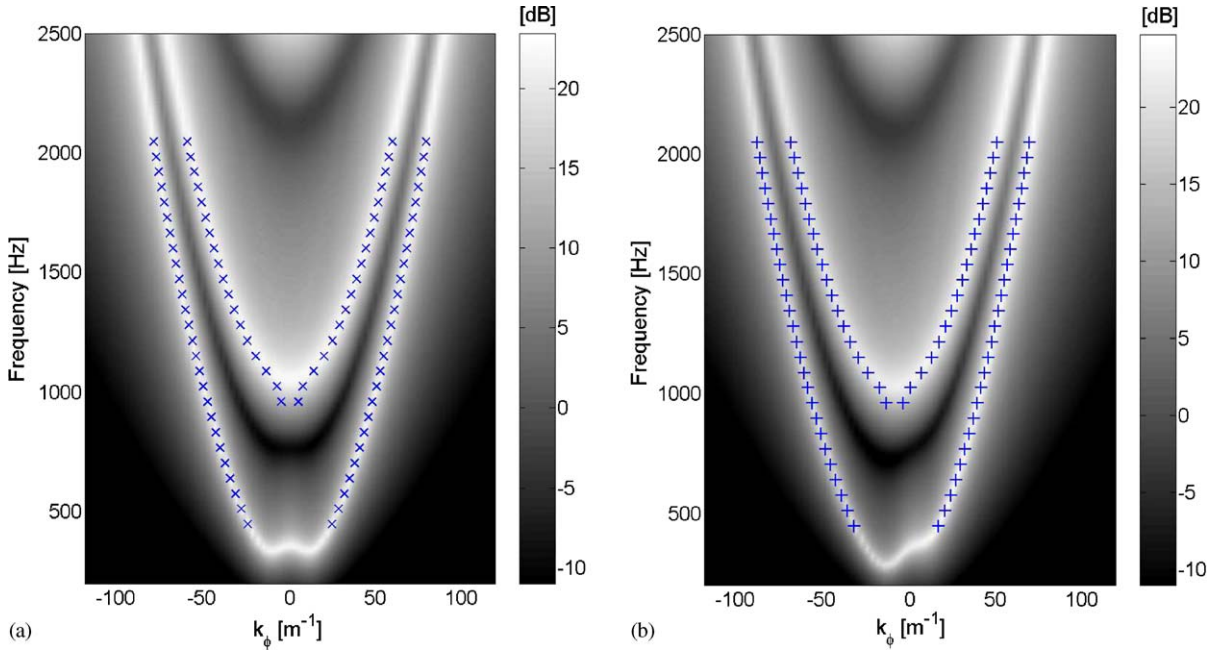

Fig. 7. Real wave numbers ($\times$ and $+$) obtained from Prony series identification when $\xi = 0.05$: (a) stationary case ($\Omega = 0$ rad/s) and (b) rotating case ($\Omega = 100$ rad/s).

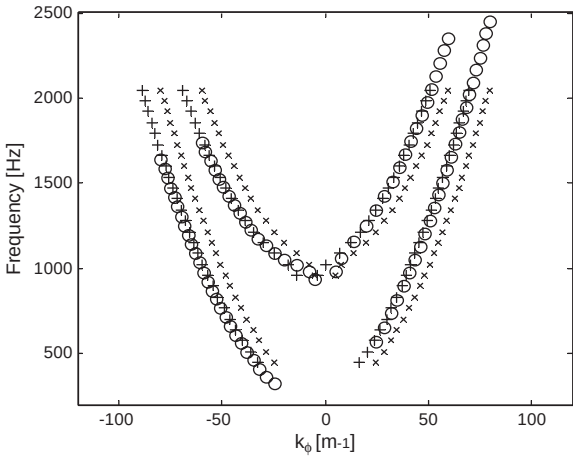

Fig. 8. Compensation of stationary dispersions relations by using Eq. (32): $\times$, stationary case, $+$, rotational case, and $\bigcirc$, compensated case.

Acknowledgements

Financial support for this work was provided by Continental Tire North America Inc., The Goodyear Tire and Rubber Company, Hankook Tire Co. Ltd., Michelin North America Co., Inc., Ford Motor Company, and Purdue University's Institute for Safe, Quiet, and Durable

Highways (funded in part by the US Department of Transportation). The authors are grateful to Farhad Tabaddor of Michelin North America Co., Inc., for suggesting that we consider the effects of rotation. The first author also thanks to Prof. W. Soedel of the Ray W. Herrick Labratories, School of Mechanical Engineering, Purdue University, for teaching him shell vibration; and for providing invaluable advice as a member of his Ph.D. examining committee.

Appendix. A: Force and moment resultants

Expressions for the normal and shear forces in local co-ordinates are given by Soedel [9]. They can also be used in Eqs. (5)–(7) described in the reference frame when the circumferential angle, θ, in local co-ordinates is replaced by the circumferential angle, ϕ, in global co-ordinates. Then the in-plane forces are expressed as

$$N_{xx} = K(\varepsilon^0_{xx} + v\varepsilon^0_{\phi\phi}), \quad N_{x\phi} = \frac{K(1-v)}{2}\varepsilon^0_{x\phi}, \quad N_{\phi\phi} = K(\varepsilon^0_{\phi\phi} + v\varepsilon^0_{xx}), \tag{A.1–A.3}$$

where the membrane strains are

$$\varepsilon^0_{xx} = \frac{\partial u_x}{\partial x}, \quad \varepsilon^0_{x\phi} = \frac{\partial u_\phi}{\partial x} + \frac{1}{a}\frac{\partial u_x}{\partial \phi}, \quad \varepsilon^0_{\phi\phi} = \frac{u_r}{a} + \frac{1}{a}\frac{\partial u_\phi}{\partial \phi}. \tag{A.4–A.6}$$

The shear forces are represented in terms of moments, i.e.,

$$Q_{xr} = \frac{\partial M_{xx}}{\partial x} + \frac{1}{a}\frac{\partial M_{x\phi}}{\partial \phi}, \quad Q_{\phi r} = \frac{\partial M_{x\phi}}{\partial x} + \frac{1}{a}\frac{\partial M_{\phi\phi}}{\partial \phi}, \tag{A.7, A.8}$$

where the moments can be expressed in terms of curvatures as

$$M_{xx} = D(\kappa_{xx} + v\kappa_{\phi\phi}), \quad M_{x\phi} = \frac{D(1-v)}{2}\kappa_{x\phi}, \quad M_{\phi\phi} = D(\kappa_{\phi\phi} + v\kappa_{xx}). \tag{A.9–A.11}$$

In Eqs. (A.9–A.11), the curvatures are expressed in terms of rotation angles as

$$\kappa_{xx} = -\frac{\partial \beta_x}{\partial x}, \quad \kappa_{x\phi} = \frac{\partial \beta_\phi}{\partial x} + \frac{1}{a}\frac{\partial \beta_x}{\partial \phi}, \quad \kappa_{\phi\phi} = \frac{1}{a}\frac{\partial \beta_\phi}{\partial \phi} \tag{A.12–A.14}$$

and

$$\beta_x = -\frac{\partial u_r}{\partial x}, \quad \beta_\phi = \frac{u_\phi}{a} - \frac{1}{a}\frac{\partial u_r}{\partial \phi}. \tag{A.15, A.16}$$

References

[1] J.S. Bolton, Y.-J. Kim, Wave number domain representation of tire vibration, *Proceedings of Inter-noise 2000*, vol. 1, 2000, pp. 184–190.
[2] Y.-J. Kim, J.S. Bolton, Modeling tire treadband vibration, *Proceedings of Inter-noise 2001*, Paper 716, 2001.
[3] S.C. Huang, W. Soedel, Effects of Coriolis acceleration on the free and forced in-plane vibrations of rotating rings on elastic foundation, *Journal of Sound and Vibration* 115 (2) (1987) 253–274.
[4] S.C. Huang, W. Soedel, Response of rotating rings to harmonic and periodic loading and comparison with the inverted problem, *Journal of Sound and Vibration* 118 (2) (1987) 253–270.

[5] S.C. Huang, W. Soedel, Effects of Coriolis acceleration on the forced vibration of rotating cylindrical shells, *Journal of Applied Mechanics* 55 (1988) 231–233.
[6] J. Padovan, Natural frequencies of rotating prestressed cylinders, *Journal of Sound and Vibration* 31 (4) (1973) 469–482.
[7] W. Kropp, Structure-borne sound on a smooth tyre, *Applied Acoustics* 26 (3) (1989) 181–192.
[8] E. Vinesse, H. Nicollet, Surface waves on the rotating tyre: an application of functional analysis, *Journal of Sound and Vibration* 126 (1) (1988) 85–96.
[9] W. Soedel, *Vibrations of Shells and Plates*, 2nd edition, Marcel Dekker Inc., New York, 1993.
[10] J.S. Bolton, H.J. Song, Y.K. Kim, Y.J. Kang, The wave number decomposition approach to the analysis of tire vibration, *Proceedings of NOISE-CON 98*, 1998, pp. 97–102.